JACS
JOURNAL OF THE AMERICAN CHEMICAL SOCIETY

Article

pubs.acs.org/JACS

Self-Supported Pd_xBi Catalysts for the Electrooxidation of Glycerol in Alkaline Media

Anna Zalineeva,[†] Alexey Serov,[‡] Monica Padilla,[‡] Ulises Martinez,[‡] Kateryna Artyushkova,[‡] Stève Baranton,[†] Christophe Coutanceau,*[,†] and Plamen B. Atanassov*[,‡]

[†]Université de Poitiers, IC2MP, UMR CNRS 7285, "Catalysis and Non-conventional Media" group, 4 rue Michel Brunet, 86073 Poitiers Cedex 9, France

[‡]Department of Chemical and Nuclear Engineering and Center for Emerging Energy Technologies, University of New Mexico, Albuquerque, New Mexico 87131, United States

ABSTRACT: Highly active self-supported Pd_xBi catalysts are synthesized by the sacrificial support method. Self-supported Pd_xBi catalysts have a porous nanostructured morphology with high surface areas (in the range from 75 to 100 $m^2\ g^{-1}$), making Pd_xBi a state-of-the-art catalyst. Pd_4Bi displays the highest activity toward glycerol oxidation. In situ Fourier transform infrared spectroscopy highlights the unique catalytic behavior of self-supported Pd_xBi materials due to their particular structure and morphology. The confinement of reactants and intermediates in pores acting as nanoreactors is responsible for the high selectivity as a function of the electrode potential: aldehyde and ketone at low potentials, hydroxypyruvate at moderate potentials, and CO_2 at high potentials. Moreover, the selectivity depends on the electrode history: it is different for the positive potential scan direction than for the reverse direction, where the catalyst becomes selective toward the production of carboxylates.

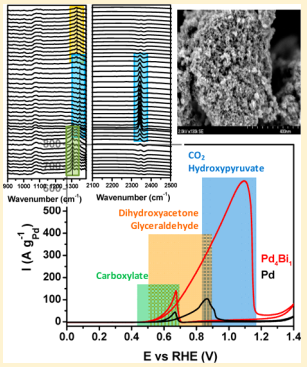

INTRODUCTION

Direct alcohol fuel cells (DAFCs) have attracted more and more interest in the recent years[1,2] as an alternative to hydrogen fed fuel cells. Alcohols are liquids, and therefore, they have high volumetric and gravimetric energy densities, their storage is easy, and their distribution does not need new infrastructures. Among alcohols, glycerol has been proposed as a convenient fuel because it has a biorenewable character,[3] and this compound is a nonvalued byproduct of the biofuel industry. For energy production the complete oxidation of glycerol into CO_2 requires the breaking of the C−C bonds, which is rather difficult to perform at the low working temperatures of DAFCs and glycerol oxidation reaction produces a large number of reaction products.[4,5] However, it has been proposed that all C3 oxidized species from glycerol are valuable fine chemicals.[6,7]

Most of alcohol electro-oxidation studies have been performed in acidic media. The majority of anode electrocatalysts developed for DAFCs working with a proton exchange membrane (namely, Nafion) used platinum based catalysts.[8,9] Platinum is known to be the most active material for the dissociative adsorption of alcohols.[10,11] In contrary, in alkaline media, Pt-free catalysts can be used in both electrodes, cathode[12,13] and anode.[14,15] Palladium based nanoalloys have indeed shown high activity and stability in alkaline media, and can be considered as possible economical substitutes of Pt for alcohol oxidation.[16−19]

The improvement of the catalytic activity and selectivity of palladium electrocatalysts is generally realized by increasing the active surface area of the catalyst and by the addition of a second metal with a promotional effect.[20,21] In the case of alcohol electro-oxidation in alkaline media, it has been shown that interactions between palladium and bismuth modified the electrocatalytic properties,[22−25] although the kind of interactions is not yet fully understood. In particular, the bismuth deposition mode and the resulting composition of the Bi deposit, the interaction with the substrate, and so forth have an impact on the activity and selectivity of the Pd modified catalysts.[26,27]

The morphology and structure of the catalytic material can also influence its catalytic behavior. Here, the synthesis by the sacrificial support method (SSM)[28−30] of hierarchically structured materials, consisting in self-supported, porous, and nanostructured Pd_xBi catalysts with different Pd/Bi atomic ratios and with high surface area, is reported. The materials are characterized by BET, SEM, TEM, EDS, and XPS to assess their microstructure, morphology and composition, and by electrochemical methods to obtain information about their surface. The activity of the catalysts toward glycerol oxidation in alkaline medium was evaluated by cyclic voltammetry. In situ FTIR spectroscopy is a very convenient method for determining the reaction products formed at the electrode/electrolyte interface, particularly because the assignment of the absorption bands was confirmed by chromatography analysis of the reaction products after chronoamperometry measurements.[7,24] This technique was thus used for studying the selectivity of the glycerol oxidation reaction as a function of the

Received: December 11, 2013
Published: February 18, 2014

   dx.doi.org/10.1021/ja412429f | J. Am. Chem. Soc. 2014, 136, 3937−3945

electrode potential. Results allow a tentative proposal of the relationship between structure−composition and electrocatalytic behavior for these materials.

EXPERIMENTAL SECTION

Synthesis of Self-Supported Pd_xBi Catalysts. A series of catalysts with various Pd:Bi ratios were prepared by the SSM, which was developed at University of New Mexico.[28−30] A known amount of silica Cab-O-Sil EH-5 (surface area ∼ 400 m^{-2} g^{-1}) was dispersed in water with an ultrasonic probe. Then, the appropriate amounts of metal precursors $Pd(NO_3)_2{\cdot}xH2O$ (metal content = 40 wt %) and $Bi(NO_3)_3$ (metal content = 42.98 wt %) from Sigma-Aldrich were added to the silica suspension. Total loading of metals on silica was calculated to be 13 wt %. The silica/precursor mixture was allowed to dry overnight. The composite materials were reduced under hydrogen atmosphere (7% H_2) at 300 °C for 2 h. After reduction, silica template was removed by etching in 7 M KOH solution and then abundantly washed with water until neutral pH was achieved. The nominal Pd to Bi atomic ratios were selected as 6:1, 4:1, and 2:1. The catalysts were denominated as Pd, Pd_6Bi, Pd_4Bi, and Pd_2Bi.

Physicochemical Characterization. The catalysts were comprehensively characterized by scanning electron microscopy (SEM; Hitachi S-5200 Nano SEM instrument with an accelerating voltage of 10 keV), transmission electron microscopy (TEM; JEOL 2010 TEM instrument with an accelerating voltage of 200 keV), energy dispersion spectroscopy (EDS), X-ray photoelectron spectroscopy (XPS; Kratos Ultra DLD spectrometer), and nitrogen adsorption (N_2-BET method using Micrometrics 2360 Gemini analyzer). SEM and TEM provided information about the morphology of samples and size of nanoparticles, while EDS and XPS were used to determine the composition of the samples for comparison with the expected composition. XPS was also used to determine the oxidation states and the eventual interactions between different elements in the materials.

Electrochemical Characterization. The inks for cyclic voltammetry (CV) experiments were prepared by dispersing 5 mg of catalyst powder with 925 μL of a water and isopropanol alcohol (4:1) mixture and 75 μL of Nafion (0.5 wt % from DuPont). Homogeneity of the inks was achieved by means of sonication using an ultrasound probe. Then, 10 μL of the mixture was applied onto a 0.2472 cm^2 geometric surface area glassy carbon disk, for a catalyst loading of 0.2 mg cm^{-2}. The electrochemical analysis of the synthesized material was performed using a Pine Instrument Company electrochemical analysis system. The cyclic voltammetry experiments were performed using a disk electrode rotated at 1300 rpm (rpm). The electrolyte was 1 M KOH saturated with N_2 at room temperature. A platinum wire and a Hg/HgO electrode were used as counter and reference electrodes, respectively, although all potentials are quoted versus the reversible hydrogen electrode (RHE). Electrocatalytic measurements were realized in 1 M KOH + 0.1 M glycerol solution at a scan rate of 0.02 V s^{-1}. The voltammograms were recorded in the range of potentials from 0.0 to 1.4 V vs RHE. The catalysts were cycled through the potential range several times until stable voltammograms were recorded. To assess the stability of materials, chronoamperometry was performed in the presence of 0.1 M glycerol for 5000 s at a potential of 0.7 V vs RHE.

In situ Fourier transform infrared (FTIR) spectroscopy (IRRAS - Nicolet 6700 FT-IR spectrometer with MCT detector) was used to gain insight into the mechanism of the glycerol electro-oxidation in alkaline media on the self-supported Pd, Pd_4Bi, and Pd_2Bi catalysts. The experimental method is described elsewhere.[30]

RESULTS

The sacrificial support method leads to self-supported bimetallic Pd_xBi materials with a spongelike structure as shown in the SEM image of Figure 1a. At higher SEM magnification, Figure 1b shows clearly that unsupported Pd_4Bi material displays nanostructured morphology. It is expected

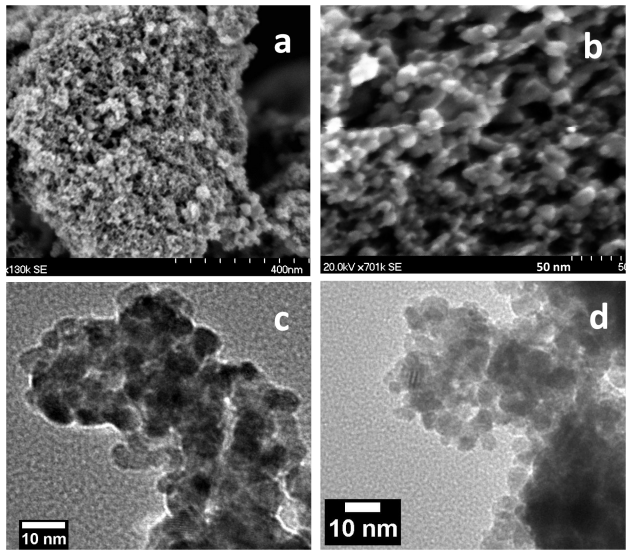

Figure 1. (a,b) SEM and (c,d) TEM micrographs for a self-supported Pd_4Bi sample.

that the presence of beads of metal delimiting pores will increase the active surface area and further will increase the catalyst utilization. This is confirmed by all catalysts presenting a well-developed 3D structure and very high surface areas determined by N_2-BET method (between 75 and 100 m^2 g^{-1}) despite moderately high temperatures for the synthesis. TEM images in Figure 1c and d also clearly show that the metal beads are composed of agglomerated nanoparticles with size of ca. 5 nm. In summary, the self-supported Pd_xBi materials prepared by SSM consist of beads of agglomerated nanoparticles with a diameter of ca. 5 nm delimiting pores with sizes from 30 to 100 nm.

Cyclic voltammograms in supporting electrolyte are presented in Figure 2. For the pure Pd material, a typical voltammogram of polycrystalline palladium is obtained, with the adsorption/absorption region of hydrogen at low potentials[31] (between 0.3 and −0.1 V) in the negative going scan, the hydrogen desorption peak in the positive going scan between −0.1 and 0.7 V, followed by the Pd surface oxide region from 0.7[24,32] to 1.4 V and in the reverse scan the reduction peak of Pd oxide species at ca. 0.6 V, according to the following equation:

$$Pd + 2OH^- = PdO + H_2O + 2e^- \quad (1)$$

Under the present experimental conditions, the electrochemical surface area (ECSA) of the pure self-supported Pd catalyst can be calculated using the method described by Grdén et al.,[32] and it was estimated at ca. 20 m^2 g_{Pd}^{-1}. This value is four to five times lower than that determined by BET, indicating the presence of microporosity nonaccessible to hydrated species. But the ESCA is of the same order than that obtained by Simões et al. with carbon supported Pd nanoparticles of 4.0 nm mean diameter,[33] which is remarkable considering that the metal is not dispersed on a high specific surface area substrate such as carbon Vulcan XC72.

The presence of bismuth clearly affects the shape of the voltammograms by limiting the hydrogen adsorption/absorption processes on palladium at low potentials, as previously observed,[34] and changing the oxidation processes at high potentials. The hydrogen adsorption/absorption processes have almost completely disappeared for the self-supported Pd_6Bi and

dx.doi.org/10.1021/ja412429f | J. Am. Chem. Soc. 2014, 136, 3937−3945

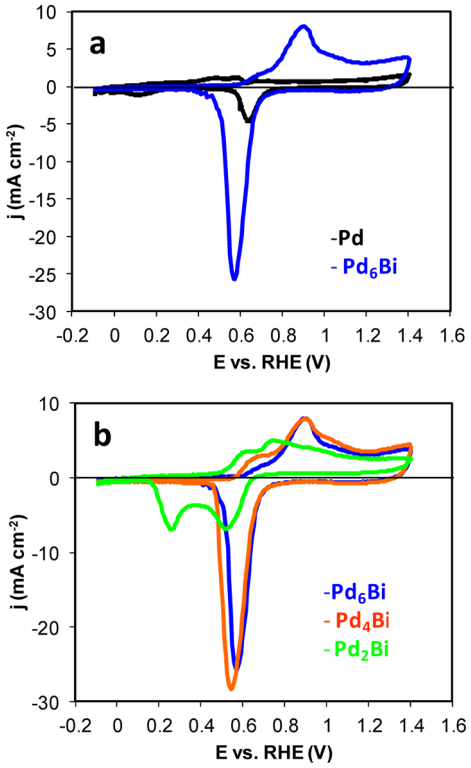

Figure 2. Cyclic voltammograms of (a) Pd and Pd_6Bi self-supported catalysts and (b) Pd_xBi self-supported catalysts, recorded in 0.1 M KOH N_2-saturated electrolyte (v = 0.020 V s^{-1}; T = 25 °C).

Pd_4Bi catalysts, indicating a high coverage of the palladium surface by bismuth atoms and strong interactions between bismuth and palladium atoms. A positive current peak related to a surface oxidation process appears with a maximum intensity located close to 0.9−0.95 V.

According to the potential-pH diagram of bismuth[35] in an aqueous medium, the Bi_2O_3 bismuth oxide phase exists as its hydrated form $Bi(OH)_3$, which is insoluble in alkaline solutions, and this latter hydrated specie can be formed as soon as 0.48 V according to the following reaction:

$$2Bi + 6OH^- = 2Bi(OH)_3 + 6e^- \quad (2)$$

In the negative going potential scan, a sharp single reduction current peak is observable between 0.55 and 0.6 V for the Pd_6Bi and Pd_4Bi catalysts with a higher intensity than for the pure Pd material. This reduction peak is attributed to the reduction of the surface oxides, including bismuth oxides[22] formed during the positive going potential scan. This suggests that bismuth redox process in Pd_6Bi and Pd_4Bi catalysts is related to the palladium redox process, and this is evidence that electronic interaction between both metals occurs. This strong interaction avoids the possibility to determine the ECSA of the Bi containing catalyst, conversely to pure Pd material, but it can reasonably be stated that it is lower than that of the pure Pd catalyst. For higher bismuth content, several oxidation/reduction peaks appeared which are due to several redox reactions of bismuth species. The reduction of oxidized Bi surface species strongly interacting with palladium occurs at higher potentials than that of oxidized Bi surface species weakly or not interacting with palladium.[23]

The XPS core level spectra of Pd 3d and Bi 4f are presented in Figure 3 for the three different Pd_xBi materials. Different

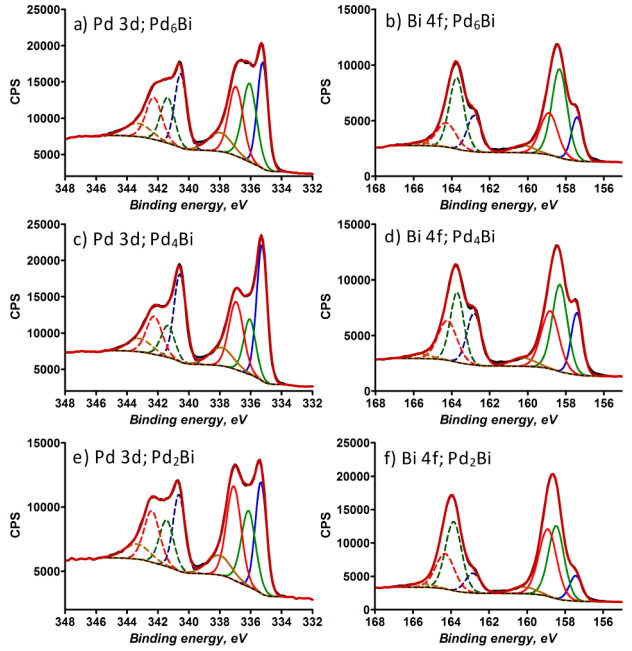

Figure 3. Detailed XPS core level spectra of Pd 3d and Bi 4f orbitals on synthesized catalysts (a,b) Pd_6Bi; (c,d) Pd_4Bi; (e,f) Pd_2Bi.

shapes of XPS spectra are obtained depending on the composition of catalyst. In Pd_xBi materials, the 3d 5/2 core level spectra of palladium were better fitted with four symmetrical peaks at ca. 335, 336, 337, and 338 eV, assigned to Pd, $Pd(OH)_x$, PdO, and PdO_2 species, respectively, as well as the 4f 7/2 core level spectra of bismuth fitted with four peaks at ca. 157, 158, 159, and 160 eV, which were attributed to Bi, $Bi(OH)_3$, BiOOH, and Bi_2O_3 species, respectively. The spectrum analysis is based on data obtained from the "Handbook of X-ray Photoelectron Spectroscopy"[36] and from previous studies by Casella and Contursi[22] on bismuth adatoms interacting with Pd surface, and also on the reasonable assumption that higher oxidation states of species lead to XPS peaks located at higher binding energies. Table 1 summarizes the main results of XPS analysis, as well as those from EDS characterization. The EDS data indicate a Pd enrichment of catalysts, whereas XPS indicated a Bi enrichment of the surface of the catalysts, but results are relatively close to the nominal atomic ratios. The EDS microanalyses carried out in several different zones of the nanostructured catalysts indicated a relatively good homogeneity of chemical composition in catalysts.

The electroactivity of the Pd_xBi catalysts toward glycerol oxidation in alkaline medium was examined by cyclic voltammetry and compared with that of a pure Pd material. At a scan rate of 20 mV s^{-1} (Figure 4a,b), an oxidation peak appears in the positive scan direction, starting from ca. 0.6 V for pure Pd material and Birich one (Pd_2Bi) and from ca. 0.5 V for Pd_6Bi and Pd_4Bi materials. The promotion effect of bismuth for glycerol oxidation is evidenced by the shift of the oxidation potential onset by ca. 100 mV toward lower potentials and by the increase of the oxidation current densities in the potential range from 0.5 to 1.2 V vs RHE. Moreover, the presence of bismuth leads to a shift of the current drop toward higher potentials, due to the slower kinetics of Pd surface oxide formation on Pd_xBi than on Pd, which will delay the surface deactivation by oxide species coverage. This clearly demon-

dx.doi.org/10.1021/ja412429f | J. Am. Chem. Soc. 2014, 136, 3937−3945

Table 1. Nominal Atomic Ratios, Atomic Ratios Determined from EDS Measurements, and Data from XPS Characterization (atomic ratios, binding energy values of XPS peaks related to Pd 3d and Bi 4f, and relative ratios of corresponding Pd and Bi species) of Self-Supported Pd_xBi Materials

nominal atom %		86/14 (6:1)		80/20 (4:1)		66/33 (2:1)	
EDS μ-analysis atom %	A1	87.1/12.9		84.5/15.5		72.4/27.6	
	A2	87.2/12.8		85/15		70.9/29.1	
	A3	86.8/13.2				70.8/29.2	
EDS atom %		87/13		84.5/15.5		71.5/28.5	
XPS atom %		75/25		73.5/26.5		61/39	
	BE (eV)[a]	atom %		BE (eV)[a]	atom %	BE (eV)[a]	atom %
XPS Pd species atom %							
Pd^0	335.2	30.7		335.2	35	335.3	25
$Pd(OH)_x$	336	25.4		335.9	24	336	23.5
PdO	336.9	26.9		336.9	29.5	337.1	36.5
PdO_2	337.8	17		338.1	11.5	338	15
XPS Bi species atom %							
Bi^0	157.4	18.6		157.4	23	157.4	10
$Bi(OH)_3$	158.4	43.9		158.3	40	158.5	53.5
BiOOH	158.8	23.3		158.8	24.5	159	26
Bi_2O_3	159.8	14.2		160	12.5	159.8	10.5

[a]Binding energy.

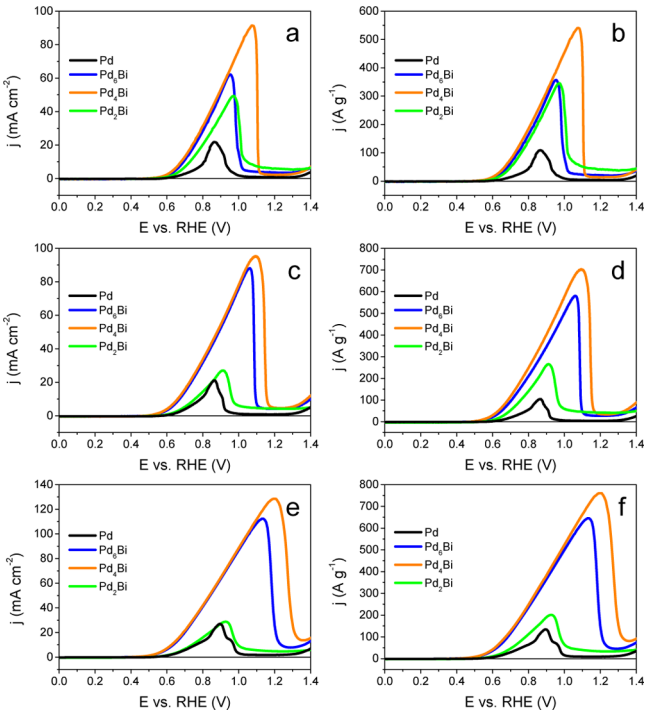

Figure 4. Polarization curves recorded for the oxidation of 0.1 M glycerol in 1 M KOH electrolyte on self-supported Pd_xBi catalysts at different scan rates: (a,b) 0.005 V s^{-1}, (c,d) 0.020 V s^{-1}, and (e,f) 0.100 V s^{-1} (T = 25 °C).

strates an increased the reaction rate of glycerol oxidation in the presence of bismuth. Under these quasi stationary experimental conditions, the following order in activity was found: Pd_4Bi > Pd_6Bi > Pd_2Bi > Pd.

Cyclic voltammetries were also performed at lower and higher scan rates (5 mV s^{-1} and 100 mV s^{-1} in Figure 4a and c, respectively). The cyclic voltammograms are very similar to those recorded at 20 mV s^{-1}, except for the current drops at high potentials which are shifted toward higher potentials when the scan rate is increased. This phenomenon of catalyst surface deactivation can be attributed to the slow kinetics of Pd surface oxide formation, which will delay the surface coverage by oxide species. No strong rate dependence in cyclic voltammograms were observed in terms of shapes and achieved peak current densities, which seems to indicate that the limitation of the reaction kinetics by diffusion of species from the bulk electrolyte toward the catalytic sites is low and that the confinement of reactant in the catalyst pores is responsible of the reaction kinetics. The behavior of the bismuth rich Pd_2Bi catalyst is different from those of the other ones: the peak current density decreases with the increase of the potential scan rate. This can be explained considering that, due to high surface coverage of the palladium surface by bismuth species, the reaction kinetics is limited in this case by the reactant adsorption process.

Chronoamperometry curves were recorded for 5000 s at 0.6 and 0.7 V in the presence of 0.1 M glycerol on different Pd_xBi catalysts (Figure 5a and b, respectively) and compared with

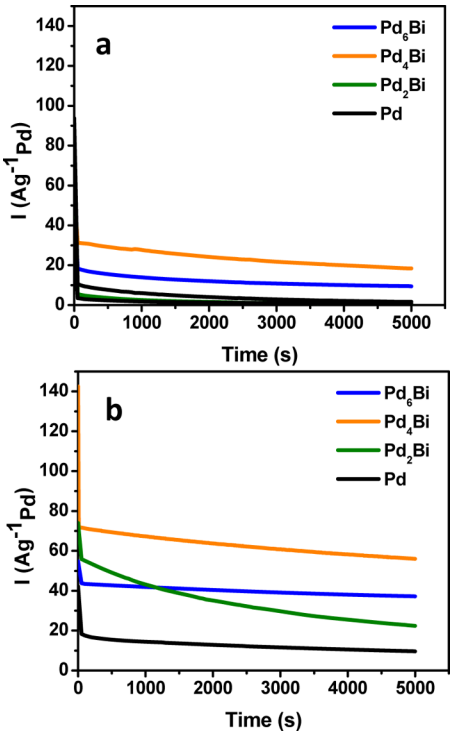

Figure 5. Chronoamperometry recorded for the glycerol electro-oxidation on a self-supported Pd and Pd_xBi catalysts at (a) 0.6 V vs RHE and (b) 0.7 V vs RHE, in 1 M KOH + 0.1 M glycerol solution (T = 25 °C).

those recorded on the pure Pd catalyst. At 0.6 V vs RHE, the currents recorded on both Pd and Pd_2Bi catalysts drop rapidly toward a value close to zero, whereas on the Pd_6Bi and Pd_4Bi catalyst the currents first decrease and stabilize at ca. 10 A g_{Pd}^{-1} and ca. 20 A g_{Pd}^{-1}, respectively, the Pd_4Bi material being the most active. At 0.7 V vs RHE, the Pd_4Bi material still remains the most active catalyst. After the initial current density of several hundreds of A g_{Pd}^{-1}, a dramatic drop of current to ca. 70 A g_{Pd}^{-1} occurs in a few seconds, likely related to capacitive

dx.doi.org/10.1021/ja412429f | J. Am. Chem. Soc. 2014, 136, 3937−3945

current decay. Then a slow decrease and the stabilization of the activity at ca. 60 A g_{Pd}^{-1} occur, which is consistent with cyclic voltammetry (Figure 4). This behavior can be attributed to the formation of adsorbed species from glycerol at the surface of the catalyst leading to decreased active surface area and decreased glycerol oxidation activity until equilibrium between adsorption of species from glycerol and desorption of reaction products is reached. These results not only highlight the higher activity of Bi containing catalysts, but also the increased stability of the Pd_4Bi material.

The in situ infrared spectra recorded on the Pd_4Bi catalyst for glycerol oxidation in alkaline medium are presented in Figure 6.

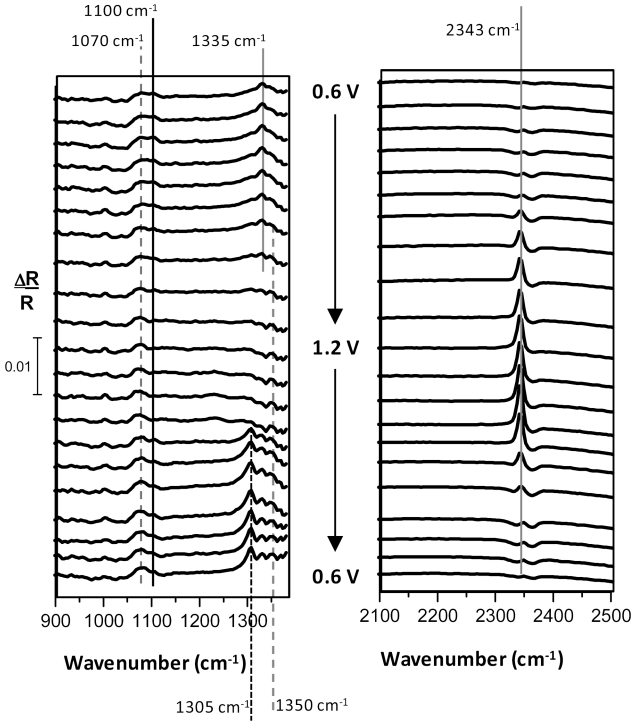

Figure 6. In situ FTIR spectra recorded for the glycerol electro-oxidation on a self-supported Pd_4Bi catalyst from 0.6 V vs RHE to 1.2 V vs RHE and to 0.6 V vs RHE in 1 M KOH + 0.1 M glycerol solution (scan rate 0.001 V s^{-1}, T = 25 °C).

The part of the spectra in the range from 1400 cm^{-1} to 2000 cm^{-1} was removed because the presence of water leads to IR absorption bands in this wavenumber region which superimpose with absorption bands of other species (such as carbonyl)[37,38] and make interpretation impossible. In the IR fingerprint region, from 1000 cm to 1400 cm^{-1}, several absorption bands can be observed. In previous works,[7,24] the assignment of the infrared absorption bands was confirmed by HPLC analysis of the reaction products after chronoamperometry experiments carried out at potentials where IR absorbed bands appeared. The first one at ca. 1070 cm^{-1} corresponds to CO stretching of aldehyde[39,40] and is observable over the whole potential range in the positive as well as in the negative scan directions. In the positive scan direction, the absorption band at 1070 cm^{-1} is accompanied from 0.6 V to ca. 0.9 V by two bands located at ca. 1100 cm^{-1} and at ca. 1335 cm^{-1}, related to CO stretching of alcohol groups and to dihydroxyacetone (DHA),[41] respectively. For potentials between 0.9 and 1.2 V, in both positive and negative scan directions, a well define absorption peak at ca. 1350 cm^{-1}, which only appeared as a shoulder for lower potentials in the positive scan direction, assigned to the formation of hydroxypyruvate,[41,42] arises simultaneously with an absorption peak at ca. 2341 cm^{-1} typical of interfacial CO_2 production.[11,40,43] At last, over the 0.9−0.6 V range in the negative scan direction, the peak of DHA at ca. 1335 cm^{-1} becomes smaller than in the positive scan direction, whereas a new absorption band at ca. 1305 cm^{-1} corresponding to carboxylate groups accompanies the one of hydroxypyruvate. Astonishingly, no absorption band located between ca. 1800 cm^{-1} and ca. 2100 cm^{-1}, which would have corresponded to bridge bonded or linear bonded CO on the noble metal surface,[44,45] has been observed over the whole studied potential range.

For comparison, the in situ infrared spectra recorded on the pure Pd and Birich Pd_2Bi catalysts for glycerol oxidation in alkaline medium are presented in Figure 7. In the case of pure Pd catalyst, only the absorption band corresponding to carboxylate groups[7,24] at ca. 1306 and 1380 cm^{-1} are present, whereas in the case of the Pd_2Bi catalyst the absorption bands related to carboxylates at ca. 1305 and 1380 cm^{-1}, and to hydroxylpyruvate at ca. 1350 cm^{-1} are observed, with different relative intensity than for the Pd_4Bi. A small absorption band can also be seen at low potentials at ca. 1335 cm^{-1} corresponding to the formation of DHA. No absorption peak at ca. 2343 cm^{-1} has been observed with both catalysts, indicating that no CO_2 is produced.

DISCUSSION

The beneficial effect of modifying palladium nanostructure by bismuth for the oxidation of alcohol,[25,46−48] and particularly glycerol,[24,26] was already pointed out. But, here it is shown that in the case of self-supported Pd_xBi materials an optimal bismuth/palladium atomic ratio of 1 to 4 leads to enhanced activity. Simões et al. observed that in the case of carbon supported Pd_xBi_{1-x}, the increase of the bismuth content in the catalyst formulation toward values higher than 10 atom % did not change the activity of the catalyst for glycerol electro-oxidation. On the basis of TEM, EDX, XRD, and electrochemical measurements, it was proposed that bismuth deposited on the carbon support formed clusters inactive for the glycerol oxidation reaction. The electrochemical characterization of Pd_xBi materials in supporting electrolyte (Figure 2) indicated that the intensity and related charge in the reduction peak at ca. 0.55 V becomes lower as the bismuth content in the material increases; the Pd and strongly interacting Pd/Bi surfaces, responsible for this reduction peak, are then smaller at high bismuth content, whereas the surface of bismuth weakly or not interacting with Pd is higher as evidenced by the reduction peak at ca. 0.2 V vs RHE. This observation can be confronted with the EDS and XPS data in Table 1 showing an enrichment of the material surface by bismuth as the Bi/Pd atomic ratio is increased. As the bismuth content is increased in the catalyst, islands or clusters of bismuth form at the palladium surface, decreasing the Pd surface available for glycerol adsorption and the interface between Pd surface and Bi surface structures, where strong interaction between both metals occurs. The order in the catalytic activity (Pd_4Bi > Pd_6B_1 > Pd_2Bi > Pd) is then due to the surface concentration of Bi. It has been proposed that the activity depended on the balance between (i) an inhibiting effect due to blocking of active sites and a catalytic effect due to enhanced adsorption of OH_{ads} on sites adjacent to Bi,[49] (ii) the amount and composition of strongly chemisorbed species and the course of electro-oxidation mechanism,[50,51] and

dx.doi.org/10.1021/ja412429f | J. Am. Chem. Soc. 2014, 136, 3937−3945

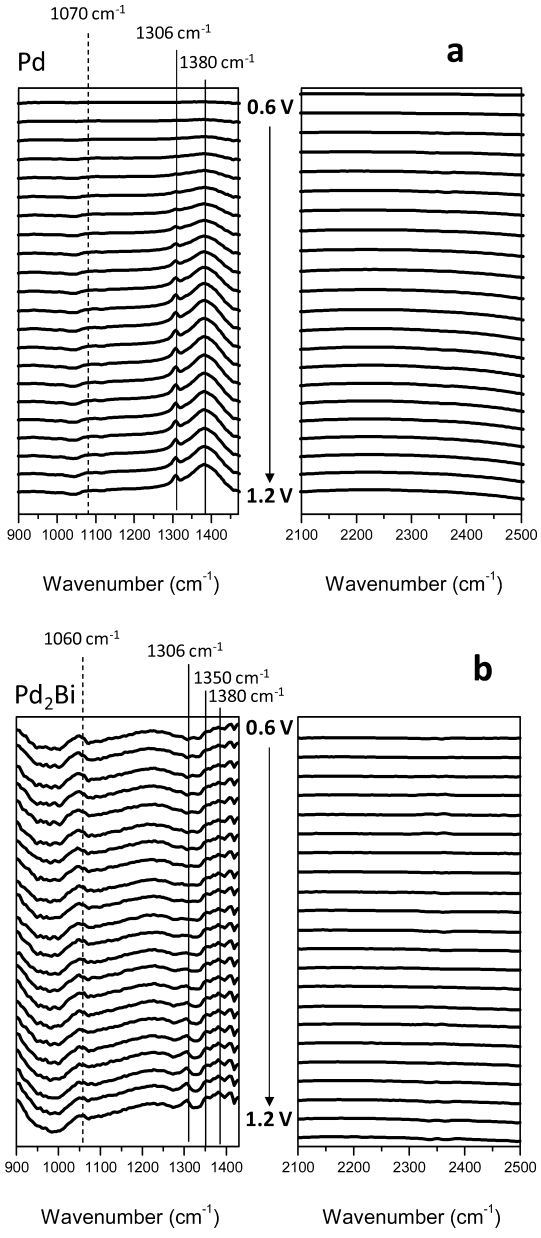

Figure 7. In situ FTIR spectra recorded for the glycerol electro-oxidation on (a) Pd and (b) Pd_2Bi self-supported catalysts from 0.6 V vs RHE to 1.2 V vs RHE in 1 M KOH + 0.1 M glycerol solution (scan rate 0.001 V s^{-1}, T = 25 °C).

(iii) the change in adsorbed species implied by the Pd surface atoms dilution by Bi surface atoms and strength of adsorption.[52] Note that all these reasons also stand for explaining the higher stability of the self-supported Pd_4Bi materials toward glycerol oxidation shown in Figure 5.

Beyond the activity, it is also known that the modification of platinum group metals surface by foreign atoms influences the selectivity of the alcohol oxidation reaction. From studies on the electro-oxidation of alcohol containing more than one carbon atom on platinum modified by adatoms, Petrii and co-workers[50,51] concluded that the presence of adatoms led to significant effects on the amount and course of electro-oxidation of strongly bonded species and that it was also possible that they affect the composition of chemisorbed species (and therefore the selectivity of the catalyst). In addition, the behavior of the most active catalyst, that is, the self-supported Pd_4Bi material, in terms of selectivity is very interesting and unique. The first important observation is its high selectivity at low overpotentials (from 0.6 V vs RHE to ca. 0.8 V vs RHE) toward low oxidized compounds, that is, glyceraldehyde (GAl) and dihydroxyaceone (DHA), as evidenced by the absorption bands at 1070 and 1335 cm^{-1}, respectively, appearing in this potential range. This indicates that the increase of activity induced by bismuth does not imply the so-called bifunctional mechanism[53] where it is proposed that surface species from alcohol adsorption are oxidatively removed thanks to the presence of surface OH species from water adsorption following a Langmuir−Hinshelwood mechanism. Indeed, the formation of aldehyde and ketone groups from alcohols does not need the addition of extra oxygen atoms, so that the enhancement of activation is due to the increased turnover frequency of reactants on the catalytic surface, possibly induced by a different adsorption mode of glycerol because Pd adsorption site dilution by bismuth atoms. Adzic also proposed that Bi adatoms prevents the adsorption and the formation of the strongly bonded intermediates which occupied multiple surface sites.[52] In acidic media, Koper et al. observed that the presence of bismuth salt in the electrolyte lowered the onset potential of oxidation on a Pt/C electrode and enhanced the turnover frequency by forming a bismuth-related active site on the surface poised for secondary alcohol oxidation.[54]

As soon as the electrode potential is increased, the formation of hydroxypyruvate (HyP) occurs as evidenced by the shoulder appearing at 1350 cm^{-1} from ca. 0.8 V vs RHE. In this case, the formation of the carboxylate function implies the addition of extra oxygen atoms and, therefore, the bifunctional mechanism. It is worth noting that, in previous works on classical carbon supported Pd and PdBi based nanocatalysts,[7,24] the formation of GAl and DHA was observed by in situ FTIR measurement and HPLC analyses, whereas the formation of HyP was not detected on such catalysts, conversely to what is observed here. Such a compound was only detected with a pure Au/C nanocatalyst.[42] It was proposed that an equilibrium between both DHA and GAl isomers existed.[24] In the case of high potentials, the oxidation reaction kinetics of a primary alcohol group toward carboxylate group becomes significantly faster than the isomerization reaction kinetics of DHA into GAl and HyP can be formed in such amount sufficient for its detection. The discrepancies between results obtained with carbon supported catalysts and self-supported materials come from the particular morphology and structure of the self-supported Pd_4Bi which are responsible of this unique behavior: the pores of size in the range from ca. 30 to 100 nm work as confined nanoreactors leading to such selectivity.

For higher potentials, the production of CO_2 evidenced by the sharp absorption band at ca. 2343 cm^{-1}, starts just after the detection of hydroxypyruvate whereas the absorption band assigned to DHA tends to disappear. Here, the breaking of the C−C bond has obviously occurred, and it is likely that in addition to CO_2, other C_1 and C_2 species are also formed, which are not detected. Indeed, the absorption peak at ca. 1240 cm^{-1} assigned to glycolate and at 1330 cm^{-1} assigned to oxalate are not present in Figure 6a. The absorption band a ca. 1400 cm^{-1} assigned to carbonate and at ca. 1577 cm^{-1} assigned to glycolate cannot be observed with the IRRAS method, because of the presence of the interfacial water absorption band which prevent the accurate determination of the other absorption bands. Again, from previous work on carbon supported

dx.doi.org/10.1021/ja412429f | J. Am. Chem. Soc. 2014, 136, 3937−3945

nanostructured Pd_xBi_y/C catalyst, no production of CO_2 was observed, and it was proposed that the dilution of Pd atoms by Bi atoms led to change the adsorption of glycerol, avoiding the breaking of the C−C bond. Here, the confined nanoreactor as proposed before can again be invoked to explain this ability to break the C−C bond at high potentials with HyP as an intermediate, according to following reactions:

$$CH_2OH{-}CO{-}COO^- + 2OH^- \rightarrow CH_2OH{-}COO^- + CO_2 + H_2O + 2e^- \quad (1)$$

and/or

$$CH_2OH{-}CO{-}COO^- + 7OH^- \rightarrow COO^-{-}COO^- + CO_2 + 5H_2O + 6e^- \quad (2)$$

and/or

$$CH_2OH{-}CO{-}COO^- + 7OH^- \rightarrow 3CO_2 + 5H_2O + 8e^- \quad (3)$$

The slow diffusion of products from the pores of the catalysts toward the bulk electrolyte leads to increased residence time in the catalytic layer, so that overoxidation of hydroxypyruvate toward CO_2 can occur. This may explain the absence of CO absorption bands although CO_2 is formed, by considering that this step related to the presence of hydroxypyruvate does not involve the formation of strongly adsorbed CO, making its further oxidation to CO_2 easier as it was proposed elsewhere in the case of ethanol electro-oxidation involving acetaldehyde intermediate at PtSn catalyst.[11,55] The formation of CO_2 can be explained by the local pH decrease; the depletion of hydroxyls species in the nanopores is a consequence of their consumption in the several electrochemical steps.

In the case of the pure Pd material, the in situ FTIR study only showed the formation of carboxylate species; the absorption bands at ca. 1335 and 1350 cm^{-1} assigned to DHA and hydroxypyruvate, respectively, were not detected. This can be explained by considering that the oxidation of glycerol occurs according to the bifunctional mechanism involving the formation of hydroxyl species at the Pd surface and reaction with adsorbed species from glycerol to give directly carboxylate species. Then, the absence of CO_2 at higher potentials is directly due to the fact that as soon as the Pd surface is oxidized, the catalyst loses its activity as evidenced by the decrease of the oxidation current in voltammograms of Figure 4. The difference in behavior between both catalysts, pure Pd and Pd_4Bi, is the delay for the formation of activated oxygenated species at the catalyst surface allowing the Langmuir−Hinshelwood mechanism to occur. Bismuth may play the role of oxygen pump protecting Pd surface from oxidation, as it was proposed to explain the better activity of PtM catalysts toward oxygen reduction reaction.[56] For Pd_2Bi, the same mechanism as for Pd_4Bi stands for low and intermediate potentials as the absorption band at 1350 cm^{-1} assigned to hydroxypyruvate formation is observed; this confirms the important role of bismuth not only toward catalytic activity but also selectivity. However, formation of carboxylate is also confirmed by the absorption bands at ca. 1306 and 1380 cm^{-1} while no CO_2 was detected at higher potentials, as for pure Pd catalyst. Again, this is related to the drop of the catalytic activity at high potentials as evidenced in Figure 4. But the reason is different than that invoked for the pure Pd catalyst. Here, the high coverage of the palladium surface by bismuth dilutes Pd surface atoms, avoiding the absorption mode leading to C−C bond breaking, and further to CO_2 formation.

Considering the use of the Pd_4Bi catalyst as anode material in an alkaline electrolysis cell, low glycerol conversion and hydrogen production rate would occur at low overvoltage, but with production of high value added ketone/aldehyde products of great interest for pharmaceutical, polymer, food, etc., industries, whereas high glycerol conversion into CO_2 and hydrogen production rate would occur at higher overvoltages, according to the following equations:

at low electrolysis cell voltages (low anode overpotentials):

$$CH_2OH{-}CHOH{-}CH_2OH \rightarrow CH_2OH{-}CO{-}CH_2OH + H_2 \quad (4)$$

and

$$CH_2OH{-}CHOH{-}CH_2OH \rightarrow CH_2OH{-}CHOH{-}CHO + H_2 \quad (5)$$

at high electrolysis cell voltages (high anode overpotentials)

$$CH_2OH{-}CHOH{-}CH_2OH + H_2O \rightarrow CH_2OH{-}CO{-}COOH + 3H_2 \quad (6)$$

and

$$CH_2OH{-}CHOH{-}CH_2OH + 3H_2O \rightarrow 3CO_2 + 7H_2 \quad (7)$$

If we consider that the oxidation of glycerol into CO_2 could also leads to the formation of other C1 and C2 species (although not detected), the number of hydrogen molecules produced per oxidized glycerol molecule should range between 3 and 7. Moreover, in all cases, the energy of hydrogen production would be at least twice to three times lower than in the case of water electrolysis, as it only depends on the electrode potential.[57] For water electrolysis, the onset potential for the anodic oxygen evolution reaction is higher than 1.23 V vs RHE (the standard water oxidation potential), whereas that for the glycerol oxidation at a Pd_4Bi catalyst is ca. 0.5 V vs RHE.

At last, it is worth noting a new absorption peak assigned to carboxylate group a ca. 1305 cm^{-1} which appears below 0.95 V in the negative potential scan direction. In this scan direction, the catalyst surface is first covered with oxide species at high potentials which can transform into hydroxide surface species as the electrode potential is lowered. These species are able to provide the extra atoms of oxygen needed for the oxidation of glycerol or adsorbed species from glycerol into carboxylate species, according to the bifunctional mechanism. In contrary, in the positive scan direction, palladium surface is most likely under reduced form at low electrode potentials and surface hydroxide species can only be formed for potentials higher than 0.7−0.8 V vs RHE, explaining the formation of aldehyde/ketone species at low potentials and hydroxypyruvate at higher potentials.

CONCLUSION

A series of highly active Pd_xBi catalysts were synthesized by the combination of the sacrificial support method and a thermal reduction process. Self-supported Pd_xBi catalysts have a porous morphology corresponding to beads of agglomerated 5 nm nanoparticles delimiting pores of 30−100 nm diameters. Such a

dx.doi.org/10.1021/ja412429f | J. Am. Chem. Soc. 2014, 136, 3937−3945

structure leads to high surface areas, in the range of 75−100 $m^2 g^{-1}$, making Pd_xBi state-of-the-art catalysts. All self-supported Pd_xBi displayed higher activity toward glycerol oxidation, confirming the promotion effect of bismuth, but the Pd_4Bi, which was found to be the most active. The most important highlights are the following: (i) The particular morphology and structure of the self-supported Pd_4Bi material leads to the formation of pores acting as nanoreactors. (ii) The confinement of reactants, intermediates, and products in the nanoreactors is responsible for the unique behavior of Pd_4Bi material in terms of selectivity for the glycerol electrooxidation as a function of the electrode potential. (iii) The selectivity is dependent on the electrode history, being different for the positive potential scan direction than for the reverse direction. (iv) In the positive potential scan direction, the catalyst is highly selective toward aldehyde and ketone at low electrode potentials. (v) At high potentials, again thanks to its particular morphology, the catalyst is able to break the C−C bond and to perform the complete oxidation of glycerol into CO_2 through hydroxypyruvate intermediate. (vi) At last, in the negative potential scan direction, the catalyst becomes selective toward the production of carboxylates.

This work represents an important demonstration that the combination of the control of the catalyst composition/morphology/structure and of the electrode potential allows orientating selectively the oxidation of alcohols, particularly glycerol, toward a given valuable product for electrosynthesis application, or toward CO_2 production for energy conversion applications (hydrogen production).

AUTHOR INFORMATION

Corresponding Authors

christophe.coutanceau@univ-poitiers.fr
plamen@unm.edu

Notes

The authors declare no competing financial interest.

ACKNOWLEDGMENTS

A.Z. thanks the Center for Emerging Energy Technologies, Farris Engineering Center (UNM) for assistance and technical support, and the county council of Poitou-Charentes (France) for financial support. UNM portion of this work was funded in part by DOE-BES EPSCoR Implementation Award: "Materials for Energy Conversion".

REFERENCES

(1) Lamy, C.; Coutanceau C. Electrocatalysis of alcohol oxidation at platinum group metals. In *Catalysis for Alcohol Fuelled Direct Oxidation Fuel Cells*; Liang, Z.-X., Zhao T. S. Eds.; RSC Energy and Science Series No. 6; Royal Society of Chemistry: Cambridge, **2012**; pp 1−70.

(2) Lai, S. C. S.; Koper, M. T. M. *Phys. Chem. Chem. Phys.* **2009**, *11*, 10446−10456.

(3) Serov, A.; Kwak, C. *Appl. Catal., B* **2010**, *97*, 1−12.

(4) Bambagioni, V.; Bevilacqua, M.; Filippi, J.; Marchionni, A.; Marchionni, A.; Moneti, S.; Vizza, F.; Bianchini, C. *Chim. Oggi* **2010**, *28*, VII−X.

(5) Bambagioni, V.; Bianchini, C.; Marchionni, A.; Filippi, J.; Vizza, F.; Teddy, J.; Serp, P.; Zhiani, M. *J. Power Sources* **2009**, *190*, 241−251.

(6) Behr, A.; Eilting, J.; Irawadi, K.; Leschinski, J.; Lindner, F. *Green Chem.* **2008**, *10*, 13−30.

(7) Simões, M.; Baranton, S.; Coutanceau, C. *ChemSusChem* **2012**, *5*, 2106−2124.

(8) Chen, A.; Holt-Hindle, P. *Chem. Rev.* **2010**, *110*, 3767−3804.

(9) Calvillo, L.; Celorrio, V.; Moliner, R.; Garcia, A. B.; Caméan, I.; Lazaro, M. J. *Electrochim. Acta* **2013**, *102*, 19−27.

(10) Hogarth, M. P.; Ralph, T. R. *Platinum Met. Rev.* **2002**, *46*, 146−164.

(11) Léger, J. -M.; Rousseau, S.; Coutanceau, C.; Hahn, F.; Lamy, C. *Electrochim. Acta* **2005**, *50*, 5118−5125.

(12) Lefèvre, M.; Proietti, E.; Jaouen, F.; Dodelet, J.-P. *Science* **2009**, *324*, 71−74.

(13) Lu, S.; Pan, J.; Huang, A.; Zhuang, L.; Lu, J. *Proc. Natl. Acad. Sci. U.S.A.* **2008**, *105*, 20611−20614.

(14) Marchionni, A.; Bevilacqua, M.; Bianchini, C.; Chen, Y. X.; Filippi, J.; Forniasero, P.; Lavacchi, A.; Miller, H.; Wang, L.; Vizza, F. *ChemSusChem* **2013**, *6*, 518−528.

(15) Ilie, A.; Simões, M.; Baranton, S.; Coutanceau, C.; Martemianov, S. *J. Power Sources* **2011**, *196*, 4965−4971.

(16) Xu, C.; Cheng, L.; Shen, P.; Liu, Y. *Electrochem. Commun.* **2007**, *9*, 997−1001.

(17) Bianchini, C.; Shen, P. K. *Chem. Rev.* **2009**, *109*, 4183−4206.

(18) Tian, N.; Zhou, Z.-Y.; Yu, N.-F.; Wang, L.-Y.; Sun, S.-G. *J. Am. Chem. Soc.* **2010**, *132*, 7580−7581.

(19) Ye, K.-H.; Zhou, S.-A.; Zhu, X.-C.; Xu, C.-W.; Shen, P. K. *Electrochim. Acta* **2013**, *90*, 108−111.

(20) Léger, J.-M.; Coutanceau, C.; Lamy, C. Electrocatalysis for the direct alcohol fuel cell. In *Fuel Cell Catalysis: a surface science approach*; Koper, M., Ed.; Wiley-VCH: Weinheim, 2009; pp 337−367.

(21) Rousseau, S.; Coutanceau, C.; Lamy, C.; Léger, J.-M. *J. Power Sources* **2006**, *158*, 18−24.

(22) Casella, I. G.; Contursi, M. *Electrochim. Acta* **2006**, *52*, 649−657.

(23) Demarconnay, L.; Brimaud, S.; Coutanceau, C.; Léger, J.-M. *J. Electroanal. Chem.* **2007**, *601*, 169−180.

(24) Simões, M.; Baranton, S.; Coutanceau, C. *Appl. Catal., B* **2011**, *110*, 40−49.

(25) Cai, J.; Huang, Y.; Guo, Y. *Electrochim. Acta* **2013**, *99*, 22−29.

(26) Zalineeva, A.; Baranton, S.; Coutanceau, C. *Electrochem. Commun.* **2013**, *34*, 335−338.

(27) Zalineeva, A.; Simões, M.; Baranton, S.; Coutanceau, C. *Int. J. Hydrogen Energy* **2013**, submitted.

(28) Serov, A.; Robson, M. H.; Artyushkova, K.; Atanassov, P. *Appl. Catal., B* **2012**, *127*, 300−306.

(29) Serov, A.; Robson, M. H.; Halevi, B.; Artyushkova, K.; Atanassov, P. *Electrochem. Commun.* **2012**, *22*, 53−56.

(30) Serov, A.; Robson, M. H.; Smolnik, M.; Atanassov, P. *Electrochim. Acta* **2013**, *109*, 433−439.

(31) Conway, B. E.; Jerkiewicz, G. *J. Electroanal. Chem.* **1993**, *357*, 47−66.

(32) Grdén, M.; Łukaszewski, M.; Jerkiewicz, G.; Czerwinski, A. *Electrochim. Acta* **2008**, *53*, 7583−7598.

(33) Simões, M.; Baranton, S.; Coutanceau, C. *J. Phys. Chem. C* **2009**, *113*, 13369−13376.

(34) Simões, M.; Baranton, S.; Coutanceau, C. *Electrochim. Acta* **2010**, *56*, 580−591.

(35) Van Muyder, J.; Pourbaix, M. *Atlas d'équilibres électrochimiques à 25 °C*; Gauthier-Villars & Cie: Paris, 1963; pp 533−539.

(36) Wagner, C. D., Riggs, W. M., Davis, L. E., Moulder, J. F., Mouilenberg, G. E., Eds. *Handbook of Xray Photoelectron Spectroscopy*; Perkin Elmer Corporation: Eden Prairie, MN, 1978; p 1.

(37) Xia, X. H.; Liess, H. -D.; Iwasita, T. *J. Electroanal. Chem.* **1997**, *437*, 233−240.

(38) Vigier, F.; Coutanceau, C.; Hahn, F.; Belgsir, E. M.; Lamy, C. *J. Electroanal. Chem.* **2004**, *563*, 81−89.

(39) Falase, A.; Main, M.; Garcia, K.; Serov, A.; Lau, C.; Atanassov, P. *Electrochim. Acta* **2012**, *66*, 295−301.

(40) Wang, L.; Meng, H.; Shen, P. K.; Bianchini, C.; Vizza, F.; Wei, Z. *Phys. Chem. Chem. Phys.* **2011**, *13*, 2667−2673.

(41) Pouchert, C. J. *The Aldrich Library of Infrared Spectra*, 3rd ed.; Aldrich Chemical Company, Inc.: Milwaukee, WI, 1981; p 1.

(42) Simões, M.; Baranton, S.; Coutanceau, C. *Appl. Catal., B* **2010**, *93*, 354−362.

(43) Dubau, L.; Hahn, F.; Coutanceau, C.; Léger, J. -M.; Lamy, C. *J. Electroanal. Chem.* **2003**, *554*−*555*, 407−415.
(44) Kunimatsu, K. *J. Electroanal. Chem.* **1982**, *140*, 205−210.
(45) Beden, B.; Hahn, F.; Juanto, S.; Lamy, C.; Léger, J.-M. *J. Electroanal. Chem.* **1987**, *225*, 215−225.
(46) Motoo, S.; Watanabe, M. *J. Electroanal. Chem.* **1979**, *98*, 203−211.
(47) Beden, B.; Kadirgan, F.; Lamy, C.; Léger, J.-M. *J. Electroanal. Chem.* **1982**, *142*, 171−190.
(48) Casado Rivera, E.; Volpe, D. J.; Alden, L.; Lind, C.; Downie, C.; VazquezAlvarez, T.; Angelo, A.; DiSalvo, F. J.; Abruna, H. *J. Am. Chem. Soc.* **2004**, *126*, 4043−4049.
(49) Schmidt, T. J.; Behm, R. J.; Grgur, B. N.; Markovic, N. M.; Ross, P. N., Jr. *Langmuir* **2000**, *16*, 8159−8166.
(50) Podlovchenko, B. I.; Petrii, O. A.; Frumkin, A. N.; Lal, H. *J. Electronal. Chem.* **1966**, *11*, 12−25.
(51) Smirnova, N. W.; Petrii, O. A.; Grzejdziak, A. *J. Electroanal. Chem.* **1988**, *251*, 73−87.
(52) Adzic, R. R. Electrocatalysis on surfaces modified by foreign metal adatoms. In *Advances in Electrochemistry and Electrochemical Engineering*; Gerisher, H., Tobias, C. W., Eds.; Wiley- Interscience: New York, 1984; Vol. *13*, pp 159−260.
(53) Watanabe, M.; Motoo, S. *J. Electroanal. Chem.* **1975**, *60*, 275−283.
(54) Kwon, Y.; Birdja, Y.; Spanos, I.; Rodriguez, P.; Koper, M. T. M. *ACS Catal.* **2012**, *2*, 759−764.
(55) Coutanceau, C.; Brimaud, S.; Dubau, L.; Lamy, C.; Léger, J.-M.; Rousseau, S.; Vigier, F. *Electrochim. Acta* **2008**, *53*, 6865−6880.
(56) Shukla, A.; Neergat, M.; Parthasarathi, B.; Jayaram, V.; Hegde, M. S. *J. Electroanal. Chem.* **2011**, *504*, 111−119.
(57) Lamy, C.; Jaubert, T.; Baranton, S.; Coutanceau, C. *J. Power Sources* **2014**, *245*, 927−936.